Solid State Sciences 154 (2024) 107612

Contents lists available at ScienceDirect

Solid State Sciences

journal homepage: www.elsevier.com/locate/ssscie

Alkali rare earth double phosphates: Promising new high temperature scintillators

Hunter B. Tisdale [a,b], Robin L. Conner [c], Luiz G. Jacobsohn [c], Hans-Conrad zur Loye [a,b,*]

[a] Center for Hierarchical Waste Form Materials, Columbia, SC, 29208, United States
[b] Department of Chemistry and Biochemistry, University of South Carolina, Columbia, SC, 29208, United States
[c] Department of Materials Science and Engineering, Clemson University, Clemson, SC, 29634, United States

A B S T R A C T

Alkali rare earth double phosphates were investigated for their X-ray induced scintillation. Double phosphates with stoichiometry $A_3Ln(PO_4)_2$ (A = K or Rb, Ln = Eu or Tb) were synthesized via a eutectic molten salt flux yielding high quality single crystals. The systematic variation of the alkali and rare earth elements in the structure allowed for insights into the effects of the chemical composition on the scintillation output. The radioluminescence of these compositions under X-ray excitation is reported with a discussion of the variance of their luminosity as a function of both the constituent alkali and lanthanide elements. The relative luminosity of $Rb_3Tb(PO_4)_2$ surpasses BGO by 30 %. The dependance of the scintillation on temperature is also investigated, including an unusual peak intensity increase for higher temperatures that can reach 1.4x of its value at room temperature for $Rb_3Tb(PO_4)_2$ at 255 °C, and 2.1x for $K_3Tb(PO_4)_2$ at 495 °C.

1. Introduction

X-ray scintillating materials, those that convert X-ray photons into ultraviolet (UV)/visible light, are of interest for numerous imaging applications, including radiography and medical computed tomography. This broad applicability of scintillators has prompted the continuing search for new materials that can effectively scintillate, where the specifics of the scintillation properties, including luminosity, thermal stability, *etc.*, ultimately determine their usefulness for specific application [1–3]. The inherent advantages of inorganic scintillators, including high density, excellent stopping power, high efficiency, and often-improved energy resolution, continue to make them an important class of materials to explore [4]. Among the broad range of materials investigated, inorganic X-ray scintillators stand out as one promising class, offering a diverse range of behaviors that make them useful for applications ranging from medical imaging to industrial non-destructive testing.

Over the years, the synthesis and characterization of crystalline scintillators has been pursued with the goal of pushing back the boundaries of performance and paving the way for applications in emerging areas and in materials science [5–18]. Previous work on alkali rare earth double phosphates focused on the fast emission of Ce-activated materials using lutetium as the rare earth to increase the stopping power for gamma-rays [19–22]. More recently, Pr^{3+} was also investigated as the activator [23]. A few other works investigated mixed alkali and other lanthanides, e.g., Sc, Y and Tb [24–26]. In this paper, we report on a new series of inorganic scintillators expanding the domain of the previously investigated materials with different rare earths and alkali element combinations. Namely, crystals of alkali rare earth double phosphates with stoichiometry $A_3Ln(PO_4)_2$ (A = K or Rb; Ln = Eu or Tb) were grown and relevant scintillation characteristics, including emission spectra, luminosity, and temperature dependence of the scintillation process, were investigated. By understanding the intricacies of these materials, particularly how their chemical composition affects their performance, we aim at contributing to the ongoing evolution of scintillators together with investigating a novel and interesting class of scintillating materials.

2. Experimental

Reagents: Eu_2O_3 (Alfa Aesar, powder, 99.99 %), $(NH_4)_2HPO_4$ (VWR, powder, 98 %), KCl (VWR, powder, 99 %), KF (Alfa Aesar, powder, 99 %), and RbCl (BTC, powder, 99 %) were used as received. RbF (Strem Chemicals, powder, 99 %) was determined by PXRD to be $HRbF_2$ and was used as received. Tb_4O_7 (Alfa Aesar, powder, 99.9 %) was heated at 1000 °C for 12 h in an alumina crucible under H_2/N_2 gas flow to reduce it to Tb_2O_3. The produced Tb_2O_3 was then used as is.

Synthesis: Single crystals of $K_3Ln(PO_4)_2$ (Ln = Eu or Tb) were synthesized via a molten flux method by utilizing a KCl/KF eutectic melt (eutectic ratio ≈ 11:9, respectively; melting point ≈ 600 °C) as a medium for crystallization. The requisite lanthanide oxide (0.5 mmol) was

* Corresponding author. Center for Hierarchical Waste form Materials, Columbia, SC, 29208, United States.
E-mail address: zurloye@mailbox.sc.edu (H.-C. zur Loye).

https://doi.org/10.1016/j.solidstatesciences.2024.107612
Received 6 May 2024; Received in revised form 18 June 2024; Accepted 19 June 2024
Available online 20 June 2024

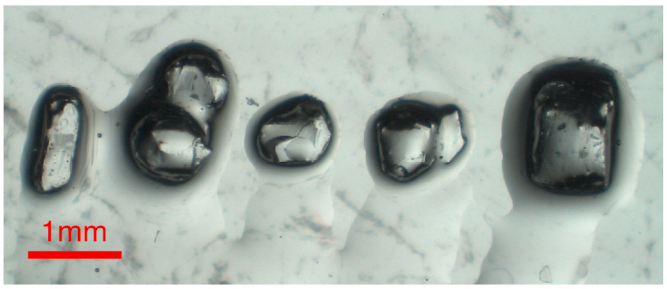

Fig. 1. Crystals of $Rb_3Tb(PO_4)_2$ suspended in immersion oil; dark portions of the crystals are due to shadows resulting from the oil, the size of the crystals, and the angle of the light.

combined and thoroughly mixed with $(NH_4)_2HPO_4$ (2 mmol) and placed into a platinum crucible. This mixture was topped with a combination of KCl (11 mmol) and KF (9 mmol) and the crucible was closed with a platinum lid. The crucible was then placed in a programmable furnace, rapidly heated to 875 °C, held at 875 °C for 12 h, cooled to 500 °C at 10 °C/h, and then rapidly cooled to room temperature by switching off the furnace. The crystals were separated from the solidified flux via sonication in deionized water for 1 h. The crystals were isolated and collected via vacuum filtration.

Single crystals of $Rb_3Ln(PO_4)_2$ (Ln = Eu or Tb) were synthesized identically to the potassium analogues with the exception of the use of a RbCl (11 mmol)/$HRbF_2$ (7.5 mmol) mixture instead of the KCl/KF mixture. The eutectic composition and melting point of RbCl/$HRbF_2$ is unknown. However, the $HRbF_2$ likely decomposes into RbF. The eutectic composition of RbCl/RbF is approximately 11:9, respectively, and melts at about 550 °C.

Powder X-ray Diffraction (PXRD): The identities and purities of the reaction products were determined via PXRD. Products were individually ground into powders using an agate mortar and pestle and powder diffraction data were collected using a Bruker D2 Phaser equipped with a LYNXEYE XE-T silicon strip detector and a sealed-tube Cu Kα anode. Diffraction patterns were measured over the 2θ range of 5°–65°. The high energy resolution of the LYNXEYE XE-T detector allowed for energy cutoff of the Kβ X-rays.

UV-Excitation Spectroscopy: A microspectrophotometer system (Olympus BX53 microscope, Horiba iHr350 spectrometer, and a free space coupled 375 nm laser) was utilized to collect UV-excited emission spectra of $Rb_3Eu(PO_4)_2$ and $Rb_3Tb(PO_4)_2$ at room temperature.

X-ray Scintillation Spectroscopy: Radioluminescence (RL) measurements were carried out using a customer-designed configuration of the Freiberg Instruments Lexsyg spectrofluorometer equipped with a Varian Medical Systems VF-50J X-ray tube with a tungsten target. The X-ray source was coupled with a Crystal Photonics CXD-S10 photodiode

Table 1
Density and scintillation results of the alkali rare earth double phosphates: density, relative luminosity to BGO, X-ray mass attenuation coefficient calculated at 40 keV, maximum relative increase of the peak intensity in relation to the corresponding value at RT and the temperature at which the maximum relative increase of the peak intensity happened.

Compound	Density (g/cm^3)	Relative luminosity to BGO	μ/ρ @ 40 keV (cm^2/g)	Maximum intensity enhancement at high temperatures	T_{max} (°C)
$K_3Eu(PO_4)_2$	3.868	0.24x	2.797	1.3x	264
$K_3Tb(PO_4)_2$	3.979	0.83x	3.051	2.1x	495
$Rb_3Eu(PO_4)_2$	4.697	0.35x	5.750	2.2x	232
$Rb_3Tb(PO_4)_2$	4.789	1.3x	5.911	1.4x	255

for continuous radiation intensity monitoring. The light emitted by the sample was collected by an Andor Technology SR-OPT-8024 optical fiber connected to an Andor Technology Shamrock 163 spectrograph coupled to a cooled (−80 °C) Andor Technology DU920P-BU Newton CCD camera (spectral resolution of ~0.5 nm/pixel). RL was measured under continuous X-ray irradiation (W characteristic lines and bremsstrahlung radiation; 40 kV, 1 mA) with an integration time of 0.5 s (Tb compounds) or 1 s (Eu compounds). The measurements with the photodiode showed the intensity of the X-rays to be stable, varying less than 1 % over time. The powdered samples filled ~8 mm diameter, 0.5 mm deep cups thus allowing for comparison and the determination of relative intensity against bismuth germanium oxide (BGO) powder [Alfa Aesar Puratronic, 99.9995 % (metals basis)] used as a reference. Relative luminosity results correspond to the ratio of the spectra integral from 300 to 750 nm using the BGO spectrum integral as reference. RL measurements, as a function of the temperature, were executed under continuous heating with a 2 °C/s heating rate and a 0.2 s (Tb compounds) or 1 s (Eu compounds) integration time. Thus, temperature increased by 0.4 or 2 °C during the acquisition of each spectrum, respectively, with spectra being acquired every 10 °C. Spectra were labeled by the starting acquisition temperature. All spectra were automatically corrected using the spectral response of the system determined by the manufacturer.

3. Results and discussion

Synthesis: Colorless and transparent crystals of all four compositions, $K_3Eu(PO_4)_2$, $K_3Tb(PO_4)_2$, $Rb_3Eu(PO_4)_2$, and $Rb_3Tb(PO_4)_2$, ranging in size from a few microns to over a millimeter across were synthesized via molten flux crystal growth. Smaller (a few microns across) crystals

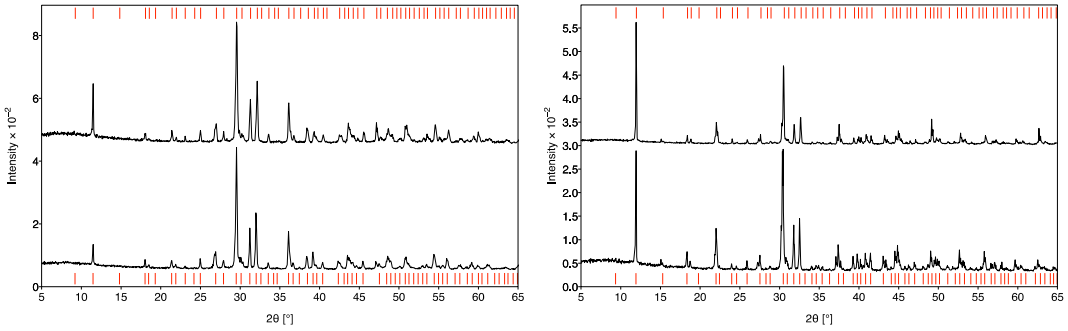

Fig. 2. Left: PXRD patterns of $Rb_3Eu(PO_4)_2$ (bottom, black) and $Rb_3Tb(PO_4)_2$ (top, black) samples used in radioluminescence measurements with calculated (CSD 2145475, 2145486) [31] peak positions for $Rb_3Eu(PO_4)_2$ (bottom, red ticks) and $Rb_3Tb(PO_4)_2$ (top, red ticks). Right: PXRD patterns of $K_3Eu(PO_4)_2$ (bottom, black) and $K_3Tb(PO_4)_2$ (top, black) samples used in radioluminescence measurements with calculated (PDF 04-016-1339, 04-023-2341) [32] peak positions for $K_3Eu(PO_4)_2$ (bottom, red ticks) and $K_3Tb(PO_4)_2$ (top, red ticks).

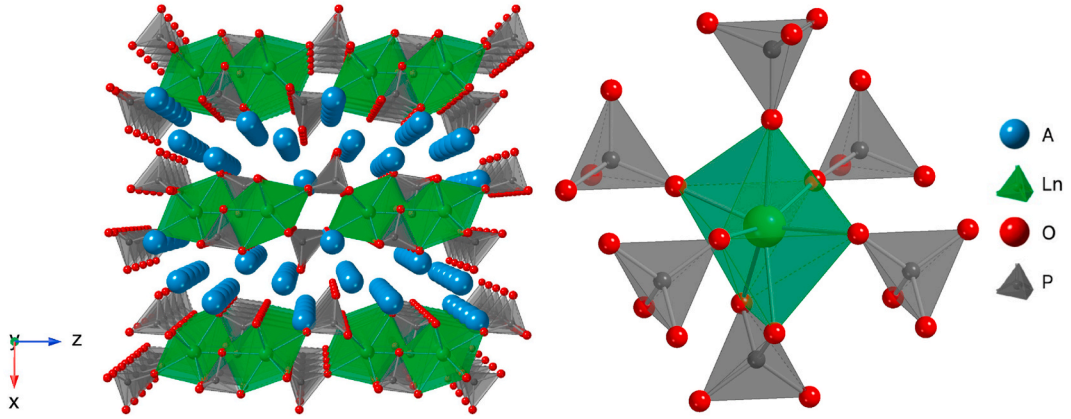

Fig. 3. Left: the room temperature, monoclinic structure of $A_3Ln(PO_4)_2$ (A = K, Rb; Ln = Eu, Tb); right: the coordination environment of Ln in high temperature, monoclinic $A_3Ln(PO_4)_2$.

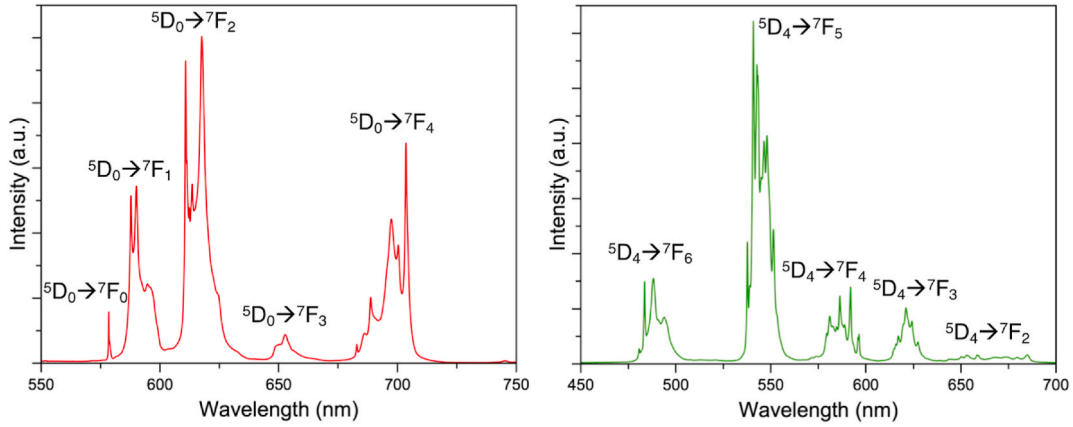

Fig. 4. Emission spectra of $Rb_3Eu(PO_4)_2$ (left) and $Rb_3Tb(PO_4)_2$ (right) under UV excitation. (λ_{exc} = 375 nm) [29].

formed with irregular shapes while larger (>1 mm across) crystals tended to be prisms with rectangular or hexagonal facets (Fig. 1).

Previously reported syntheses of alkali rare earth phosphate crystals with stoichiometry $A_3Ln(PO_4)_2$ (A = alkali metal, Ln = lanthanide) typically employed a high-temperature flux as the crystal growth medium, although the fluxes used varied considerably. Alkali carbonates, pyrophosphates, chlorides, fluorides, and chloride-fluoride mixtures have all been used to obtain single crystals [21,27–29]. The potassium or rubidium chloride-fluoride mixture was chosen in this study for their ability to solubilize the lanthanide oxides, the consequential abundance of the alkali element, the ease of separating the products from the flux (via sonication in water), and the lowered melting temperature of the chloride-fluoride mixture via the formation of a eutectic. PXRD measurements were used to confirm the identity of these materials (Fig. 2). Density values calculated from single crystal XRD data are shown in Table 1, where the density of $Rb_3Tb(PO_4)_2$ is found to be similar to that of $(Y,Gd)_2O_3$:Eu [30].

All four compositions are isostructural and crystallize in the monoclinic space group $P2_1/m$. The structure consists of 2D layers of 7-coordinate LnO_7 monocapped trigonal prisms interconnected by PO_4

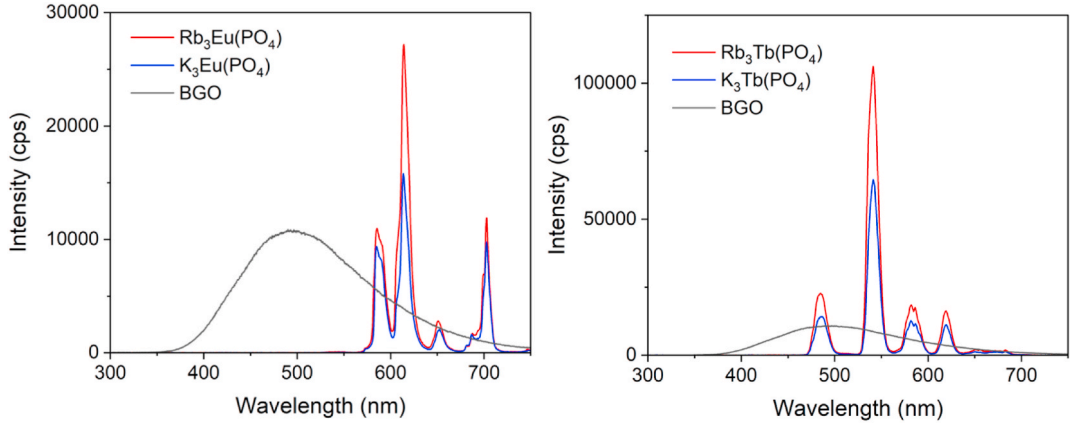

Fig. 5. X-ray scintillation emission spectra of the alkali rare earth double phosphates (Rb = red, K = blue) and BGO (black).

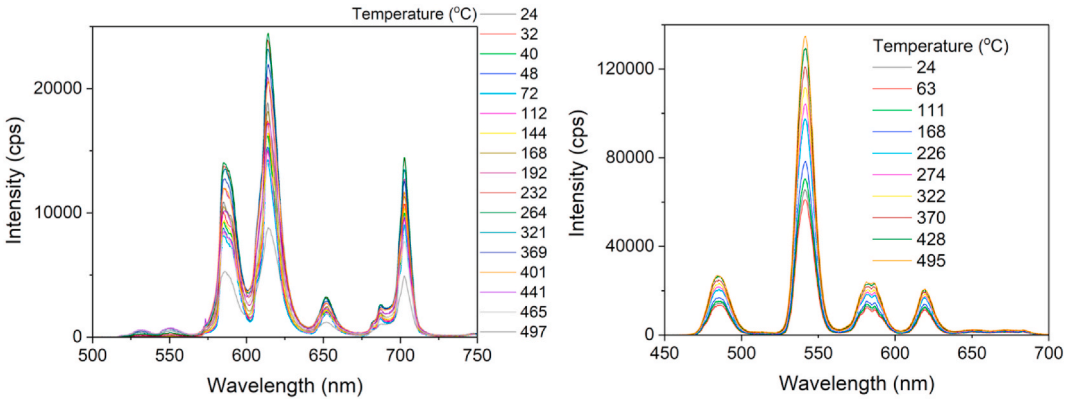

Fig. 6. Scintillation spectra at different temperatures of $K_3Eu(PO_4)_2$ (left) and $K_3Tb(PO_4)_2$ (right).

tetrahedra (Fig. 3). Each Ln atom is coordinated by five monodentate phosphates and one bidentate phosphate. These $Ln(PO_4)_2$ layers are separated by layers of alkali atoms with a Ln-Ln distance between layers ranging from about 7.4 Å for the K-containing structures to about 7.7 Å for the Rb-containing structures.

X-ray Scintillation: The choice of rare earth, its interaction with the host lattice, and the overall X-ray absorptivity per unit of volume influence the overall light output, and tuning these parameters presents opportunities for optimizing scintillation output. Since the title phases are all isostructural at room temperature, the X-ray scintillation investigation of this series of alkali rare earth double phosphates, specifically $K_3Eu(PO_4)_2$, $K_3Tb(PO_4)_2$, $Rb_3Eu(PO_4)_2$, and $Rb_3Tb(PO_4)_2$, was designed to yield insight into the influence of chemical composition on variations of the scintillation performance. First, we note that the luminescence of these double phosphates was attributed to the rare earth in their chemical composition, Eu^{3+} and Tb^{3+}. Alkali mixed rare earth double phosphates $K_3Tb_{1-x}Eu_x(PO_4)_2$ and $K_3Gd_{1-x}Eu_x(PO_4)_2$ also showed rare earth luminescence [24]. Moreover, several commercially available scintillators are intrinsic, $CdWO_4$ and BGO, including a rare earth based scintillator, $CeBr_3$. Fig. 4 shows the photoluminescence spectra of the double phosphates under UV excitation where the $^5D_0 \rightarrow {}^7F_J$, with J = 1, 2, 3 and 4, Eu^{3+} transitions [33] (left) and the $^5D_4 \rightarrow {}^7F_J$, with J = 6, 5, 4 and 3, Tb^{3+} transitions (right) [34] can be seen.

The scintillation spectra obtained under X-ray excitation are shown in Fig. 5. The same rare earth transitions revealed under UV excitation were observed under X-ray excitation. Also shown are the results of the measurements of the BGO powder. These measurements were used to determine the relative luminosity of the double phosphates. Noticeably, the peak intensities of the Rb analogues were higher than that of the K analogues. A significant difference in performance was found between Eu and Tb: both Tb containing compositions scintillated significantly more intensely than the two Eu containing analogues. All of the double phosphates had maximum peak intensities greater than the maximum intensity observed for BGO. These differences were quantified in terms of the relative luminosity that yielded the following results: $K_3Eu(PO_4)_2$ = 0.24x BGO, $Rb_3Eu(PO_4)_2$ = 0.35x BGO, $K_3Tb(PO_4)_2$ = 0.83x BGO, and $Rb_3Tb(PO_4)_2$ = 1.3x BGO (Table 1). For comparison, the absolute luminosity of a $CdWO_4$ single crystal is 1.8x that of a BGO single crystal [35]. From these values, the following ratios were extracted: for the K series, the relative luminosity increased by a factor of 0.83/0.24 = 3.46x from Eu to Tb, and for the Rb series it increased by a factor of 3.71x. For the Eu series, the relative luminosity increased by a factor of 0.35/0.24 = 1.46x from K to Rb, and for the Tb series it increased by a factor of 1.57x. These results can be approximated to be 1.5x from K to Rb, and 3.6x from Eu to Tb.

Scintillation intensity is determined by the number of X-rays absorbed by the scintillator times the number of UV–visible light photons generated by each absorbed X-ray. The absorption of X-rays was estimated in terms of the X-ray mass attenuation coefficient $\mu/\rho = \sum_i w_i \left(\mu/\rho\right)_i$, where w_i is the fraction by weight of the ith atomic constituent, and $\left(\mu/\rho\right)_i$ are the elemental mass attenuation coefficients obtained from the NIST database [36]. For simplicity, the mass attenuation coefficient was calculated for the maximum X-ray energy used in our experiments, 40 keV; the X-ray mass attenuation coefficient values obtained are shown in Table 1. From Eu to Tb, the mass attenuation coefficient barely changed by 1.06x. On the other hand, from K to Rb, it changed by a factor of 2x. Overall, the results above agreed with the relative luminosity results, *i.e.*, an increase in the atomic number, Z, resulted in higher X-ray absorption and thus a higher scintillation output. Given all the approximations and experimental uncertainties, the 1.5x enhancement of the scintillation output from K to Rb was essentially attributed to the increase in X-ray absorption as reflected in the 2x increase of the X-ray mass attenuation coefficient. However, the 3.6x increase in luminosity from Eu to Tb against the quite small change of the X-ray mass attenuation coefficient (1.06x) suggested that other factors must be evoked to explain these results. Further discussion below will focus on the change from Eu to Tb.

The scintillation efficiency is known to depend on the efficiency of conversion of the incoming X-ray photon in generating electron-hole pairs, the transport efficiency of the charge carriers through the structure of the scintillator, and the efficiency of the luminescence center, in this case the rare earths [37]. The conversion efficiency is related to the band gap, decreasing for higher band gap values: $\sim E_{Xray}/2.3E_{gap}$, where E_{Xray} is the energy of the X-ray; the transport efficiency is sensitive to the presence of defects that can trap charge carriers (*e.g.*, anionic vacancies); and the efficiency of the luminescence center is sensitive to the presence of quenching defects in its vicinity [38]. Unfortunately, the band gap values of the double phosphates being investigated are not known. Nevertheless, the band gap of the $K_3Ln(PO_4)_2$ series with Ln = Y, L and Gd only slightly decreased (~5 %) from 8.39 eV (for Y and La) to 8.07 eV (for Gd) [28]. These results suggested that the band gap of the alkali rare earth double phosphates is not significantly sensitive to the nature of the rare earth and thus unlikely to be responsible for the 3.6x enhancement of the scintillation output. Due to the shielded nature of the 4*f*-4*f* electronic transitions involved in the luminescence of the rare earths Eu^{3+} and Tb^{3+}, the luminescence efficiency of these ions is expected to be high and rather insensitive to the local structure. On the other hand, the long lifetime of these forbidden transitions facilitates energy transfer. Additional factors such as the proximity of the rare earth excited state to the edge of the conduction band and the existence of other electronic states close to the excited state can lead to reduced radiative recombination. Presently, our results cannot suggest the origin of the enhancement of the scintillation efficiency. Further analysis is hindered since the efficiency of the charge carrier transport is derived from the efficiencies

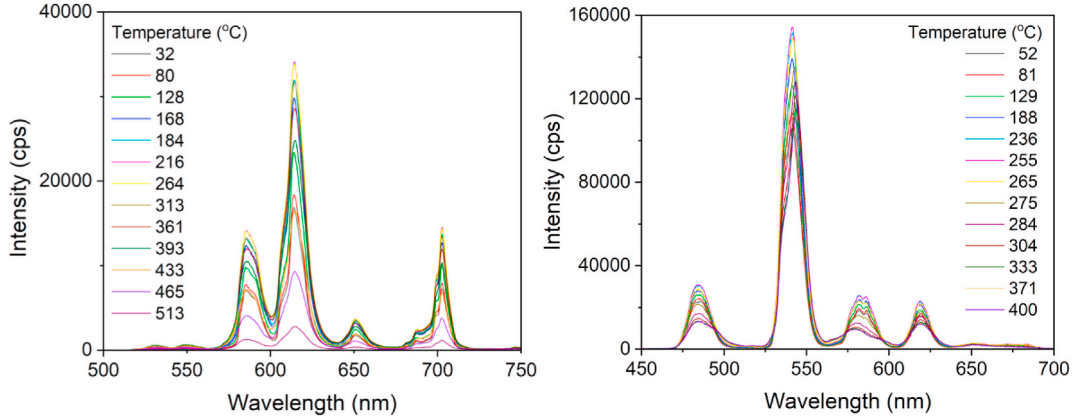

Fig. 7. Scintillation spectra at different temperatures of $Rb_3Eu(PO_4)_2$ (left) and $Rb_3Tb(PO_4)_2$ (right).

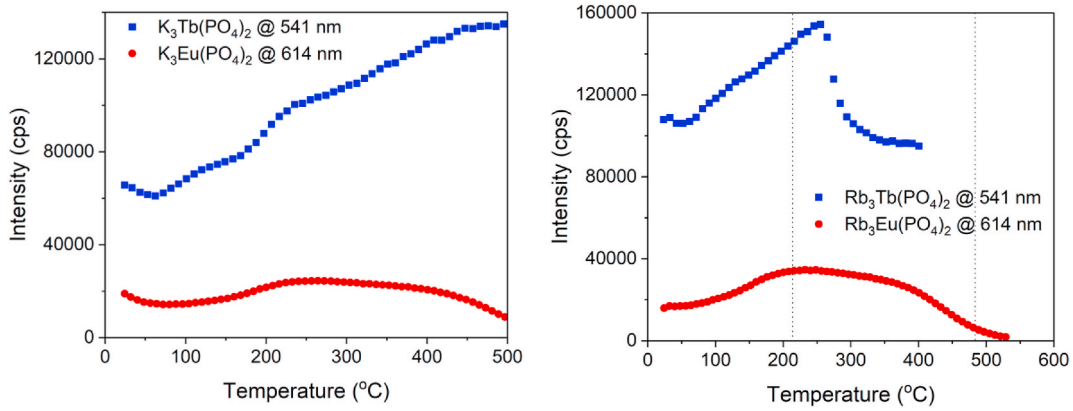

Fig. 8. Scintillation peak intensity versus temperature of the alkali rare earth double phosphates with known structure transitions shown as dotted vertical lines.

of electron-hole pair generation, of the luminescence center, and of the total efficiency of the scintillator [37], and these quantities are not known. In addition to the above, it is also important to take into consideration the possibility of rare earth concentration quenching. The investigation of $K_3Tb_{1-x}Eu_x(PO_4)_2$ with x = 0.05, 0.1 and 0.2 suggested concentration quenching already at these low Eu concentrations [24]. Consequently, in our samples where Eu or Tb is at full content (*i.e.*, x = 1), concentration quenching should be expected. Unfortunately, presently, the effect of Tb concentration has not been investigated in alkali rare double phosphates and thus it is not possible to account for this effect in a more quantitative way nor to compare its magnitude for Eu and Tb. Likely, besides changes in the X-ray absorption efficiency mostly by changing from K to Rb, rare earth concentration quenching plays a relevant role in determining the final scintillation output.

The efficiency of most scintillating materials exhibits a strong temperature dependency due to thermal quenching effects, changes of lattice parameters, or even crystal structure transitions [39,40]. To investigate the temperature dependence of the X-ray scintillation of the alkali rare earth double phosphates, all four compositions were heated *in situ* with intermittent collections of their scintillation spectra under

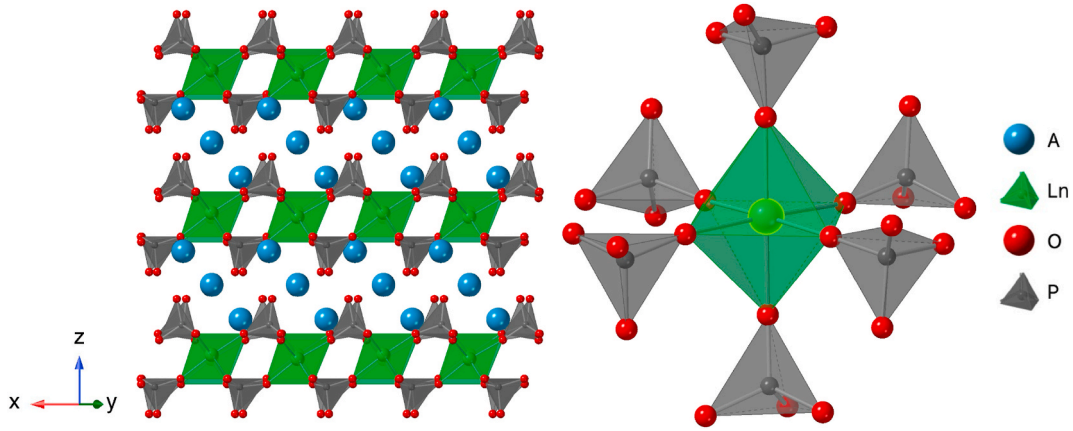

Fig. 9. Left: the high temperature, trigonal structure of $A_3Ln(PO_4)_2$ (A = K, Rb; Ln = Eu, Tb); right: the coordination environment of Ln in high temperature, trigonal $A_3Ln(PO_4)_2$.

continuous X-ray excitation at different temperatures (Figs. 6 and 7).

Of particular interest was the temperature dependence of the scintillation output of each composition, as shown in the plots of maximum peak intensity vs temperature, Fig. 8. For the Tb-based scintillators, scintillation intensity was evaluated at 541 nm that corresponds to the $^5D_4 \rightarrow {}^7F_5$ Tb^{3+} transition, and for the Eu-based scintillators at 614 nm that corresponds to the $^5D_0 \rightarrow {}^7F_2$ Eu^{3+} transition. Interestingly, all materials presented an increase of scintillation output with the increase of temperature, some of which could be attributed to the contribution of thermally stimulated luminescence as observed in other scintillators [40]. Table 1 summarizes the scintillation enhancement due to the increase of temperature in terms of the highest intensity relative to the intensity at RT and the temperature at which it happens. Worthy of note is the 2.1x enhancement in scintillation peak intensity $K_3Tb(PO_4)_2$ achieved at 495 °C in relation to its value at RT, and the 1.4x enhancement of the scintillation peak intensity of the brightest scintillator $Rb_3Tb(PO_4)_2$ at 255 °C. The specific scintillation behavior as a function of the temperature was material dependent and is discussed below. For $K_3Eu(PO_4)_2$ and $Rb_3Eu(PO_4)_2$, the same general curve shape is observed. Both exhibit an increase in scintillation intensity between 100 and 200 °C, a slow decrease until about 400 °C, and a steady decrease from 400 °C to higher temperatures with no sudden changes in slope in either curve. For $K_3Tb(PO_4)_2$, its scintillation increases at a nearly constant rate for the majority of the temperature range with only a slight decrease between room temperature and ~60 °C. At about 450 °C, the onset of a trend for saturation can be seen. $Rb_3Tb(PO_4)_2$ demonstrates a similar behavior of scintillation, decreasing up to ~50 °C followed by a nearly constant rate increase with temperature but with one notable difference: a sharp drop in intensity at approximately 255 °C which slowly plateaus at a value slightly below its room temperature value.

It was previously reported that the K and Rb rare earth double phosphates, which crystallize in the monoclinic space group $P2_1/m$, experience a thermally induced structure transition to the trigonal space group $P31\,m$ at a temperature specific to each composition [27,29,41]. This change arises from a reduction in denticity of one the of phosphate groups surrounding the rare earth atoms (bidentate to monodentate) [29]. This changes the geometry of the rare earth polyhedra from monocapped trigonal prismatic (CN = 7, noncentrosymmetric, Fig. 3) to octahedral (CN = 6, centrosymmetric, Fig. 9). The Rb analogues tend to transition at lower temperatures than the K analogues and while the transition temperatures of the K analogues were outside of the range of the *in situ* heating stage used, the transition temperatures for $Rb_3Eu(PO_4)_2$ and $Rb_3Tb(PO_4)_2$ were attainable. Their transition temperatures are marked as vertical lines in Fig. 8. For $Rb_3Eu(PO_4)_2$, the transition temperature occurs very near the highest temperature measured and no sudden change in the intensity is observed. However, the sharp decline in the intensity curve for $Rb_3Tb(PO_4)_2$ occurs within 40 °C above the expected transition temperature (215 °C) and is most likely caused by the aforementioned structure transition. Assuming this drop in intensity is indeed caused by the structure transition to the trigonal space group, then a positive correlation between scintillation efficiency and temperature only appears to occur for the Tb analogues in the monoclinic structure.

4. Summary and conclusions

A series of inorganic scintillators, the alkali rare earth double phosphates with stoichiometry $A_3Ln(PO_4)_2$ (A = K or Rb; Ln = Eu or Tb), were analyzed with respect to their scintillation behavior. Among them, $Rb_3Tb(PO_4)_2$ surpassed BGO in total X-ray scintillation luminosity by 30 %. The temperature dependence of the scintillation for these compositions showed an enhancement for higher temperatures whose behavior depended on the chemical composition. While a 1.4x enhancement of the peak intensity of the brightest scintillator $Rb_3Tb(PO_4)_2$ was reached at 255 °C, the peak intensity of $K_3Tb(PO_4)_2$ was enhanced by 2.1x at the impressive temperature of 495 °C. Overall, the high luminosity and unique thermal properties of these compounds make them attractive new scintillators deserving of further investigation.

CRediT authorship contribution statement

Hunter B. Tisdale: Writing – original draft, Investigation, Conceptualization. **Robin L. Conner:** Writing – review & editing, Investigation, Formal analysis. **Luiz G. Jacobsohn:** Writing – review & editing, Funding acquisition, Formal analysis. **Hans-Conrad zur Loye:** Writing – review & editing, Funding acquisition, Conceptualization.

Declaration of competing interest

The authors declare that they have no known competing financial interests or personal relationships that could have appeared to influence the work reported in this paper.

Data availability

Data will be made available on request.

Acknowledgments

Research was conducted by the Center for Hierarchical Waste Form Materials (CHWM), an Energy Frontier Research Center (EFRC). Research was supported by the U.S. Department of Energy, Office of Basic Energy Sciences, Division of Materials Sciences and Engineering under Award DE-SC0016574. Material synthesis, structural characterization and luminescence measurements were performed at USC. The work by R.L. Conner and L.G. Jacobsohn was supported by the NSF under grant no. DMR-1653016. Scintillation measurements were performed at Clemson University.

References

[1] C. Ronda, H. Wieczorek, V. Khanin, P. Rodnyi, Review—scintillators for medical imaging: a tutorial overview, ECS J. Solid State Sci. Technol. 5 (2016) R3121–R3125.
[2] C.W.E. van Eijk, Inorganic scintillators in medical imaging, Phys. Med. Biol. 47 (2002) R85–R106.
[3] C.W.E. van Eijk, Inorganic scintillators in medical imaging detectors, Nucl. Instrum. Methods Phys. Res., Sect. A 509 (2003) 17–25.
[4] M. Nikl, A. Yoshikawa, Recent R&D trends in inorganic single-crystal scintillator materials for radiation detection, Adv. Opt. Mater. 3 (2015) 463–481.
[5] G.B. Ayer, V.V. Klepov, M.D. Smith, M. Hu, Z. Yang, C.R. Martin, G. Morrison, H.-C. zur Loye, $BaWO_2F_4$: a mixed anion X-ray scintillator with excellent photoluminescence quantum efficiency, Dalton Trans. 49 (2020) 10734–10739.
[6] G.B. Ayer, M.D. Smith, L.G. Jacobsohn, G. Morrison, H.B. Tisdale, L.S. Breton, W. Zhang, P.S. Halasyamani, H.-C. zur Loye, Synthesis of hydrated ternary lanthanide-containing chlorides exhibiting X-ray scintillation and luminescence, Inorg. Chem. 60 (2021) 15371–15382.
[7] G.B. Ayer, G. Morrison, M.D. Smith, L.G. Jacobsohn, H.-C. zur Loye, Luminescence and scintillation of $[Nb_2O_2F_9]^{3-}$-dimer-containing oxide-fluorides: $Cs_{10}(Nb_2O_2F_9)_3F$, $Cs_{9.4}K_{0.6}(Nb_2O_2F_9)_3F$, and $Cs_{10}(Nb_2O_2F_9)_3Cl$, Inorg. Chem. 61 (2022) 3256–3262.
[8] A.A. Berseneva, L.W. Masachchi, L.G. Jacobsohn, H.-C. zur Loye, Tunable salt-inclusion chalcogenides for ion exchange, photoluminescence, and scintillation, Chem. Mater. 35 (2023) 1417–1431.
[9] D. Carone, L.G. Jacobsohn, L.S. Breton, H.-C. zur Loye, Synthesis, structure, and scintillation of $Rb_4Ta_2Si_8O_{23}$, Solid State Sci. 127 (2022) 106861.
[10] W. Gao, G. Niu, L. Yin, B. Yang, J.-H. Yuan, D. Zhang, K.-H. Xue, X. Miao, Q. Hu, X. Du, J. Tang, One-dimensional all-inorganic K_2CuBr_3 with violet emission as efficient X-ray scintillators, ACS Appl. Electron. Mater. 2 (2020) 2242–2249.
[11] C. Hu, L. Zhang, R.-Y. Zhu, M. Demarteau, R. Wagner, L. Xia, J. Xie, X. Li, Z. Wang, Y. Shih, T. Smith, Ultrafast inorganic scintillator-based front imager for Gigahertz Hard X-ray imaging, Nucl. Instrum. Methods Phys. Res., Sect. A 940 (2019) 223–229.
[12] V. Kumar, Z. Luo, A review on X-ray excited emission decay dynamics in inorganic scintillator materials, Photonics 8 (2021) 71.
[13] L. Lu, M. Sun, T. Wu, Q. Lu, B. Chen, B. Huang, All-inorganic perovskite nanocrystals: next-generation scintillation materials for high-resolution X-ray imaging, Nanoscale Adv. 4 (2022) 680–696.
[14] G. Morrison, A.M. Latshaw, N.R. Spagnuolo, H.-C. zur Loye, Observation of intense X-ray scintillation in a family of mixed anion silicates, $Cs_3RESi_4O_{10}F_2$ (RE = Y, Eu-

Lu), obtained via an enhanced flux crystal growth technique, J. Am. Chem. Soc. 139 (2017) 14743.
[15] K.S. Pestovich, L. Stand, C.L. Melcher, E. Van Loef, M. Zhuravleva, Crystal growth of new high light yield halide perovskite scintillator $RbSrI_3$, J. Cryst. Growth 627 (2024) 127540.
[16] Y. Wang, Y. Wang, X. Dai, W. Liu, X. Yin, L. Chen, F. Zhai, J. Diwu, C. Zhang, R. Zhou, Z. Chai, N. Liu, S. Wang, Inorganic X-ray scintillators based on a previously unnoticed but intrinsically advantageous metal center, Inorg. Chem. 58 (2019) 2807–2812.
[17] X. Zhao, G. Niu, J. Zhu, B. Yang, J.-H. Yuan, S. Li, W. Gao, Q. Hu, L. Yin, K.-H. Xue, E. Lifshitz, X. Miao, J. Tang, All-inorganic copper halide as a stable and self-absorption-free X-ray scintillator, J. Phys. Chem. Lett. 11 (2020) 1873–1880.
[18] F. Zhou, Z. Li, W. Lan, Q. Wang, L. Ding, Z. Jin, Halide perovskite, a potential scintillator for X-ray detection, Small Methods 4 (2020).
[19] L.A. Boatner, L.A. Keefer, J.M. Farmer, D. Wisniewski, A.J. Wojtowicz, Cerium-activated rare-earth orthophosphate and double-phosphate scintillators for x- and gamma-ray detection, SPIE Proc. 5540 (2004) 73–87.
[20] D. Wisniewski, A.J. Wojtowicz, W. Drozdowski, J.M. Farmer, L.A. Boatner, $Rb_3Lu(PO_4)_2$:Ce and $Cs_3Lu(PO_4)_2$:Ce – new promising scintillator materials, Cryst. Res. Technol. 38 (2003) 275–282.
[21] D. Wisniewski, A.J. Wojtowicz, W. Drozdowski, J.M. Farmer, L.A. Boatner, Scintillation and luminescence properties of Ce-activated $K_3Lu(PO_4)_2$, J. Alloys Compd. 380 (2004) 191–195.
[22] D. Wisniewski, A.J. Wojtowicz, L.A. Boatner, Properties of Ce-activated alkali-lutetium double phosphate scintillators, Radiat. Meas. 45 (2010) 400–402.
[23] M. Trevisani, K.V. Ivanovskikh, F. Piccinelli, M. Bettinelli, Fast 5d-4f luminescence in Pr^{3+}-doped $K_3Lu(PO_4)_2$, J. Lumin. 152 (2014) 2–6.
[24] V.B. Mikhailik, H. Kraus, P. Dorenbos, Efficient VUV sensitization of Eu^{3+} emission by Tb^{3+} in potassium rare-earth double phosphate, Phys. Status Solidi RRL 3 (2009) 13–15.
[25] J.S. Neal, L.A. Boatner, M. Spurrier, P. Szupryczynski, C.L. Melcher, Cerium-doped mixed-alkali rare-earth double-phosphate scintillators for x- and gamma-ray detection, SPIE Proc. 6319 (2006) 631907.
[26] J.S. Neal, L.A. Boatner, M. Spurrier, P. Szupryczynski, C.L. Melcher, Cerium-doped mixed-alkali rare-earth double-phosphate scintillators for thermal neutron detection, Nucl. Instrum. Methods Phys. Res., Sect. A 579 (2007) 19–22.
[27] J.M. Farmer, L.A. Boatner, B.C. Chakoumakos, C.J. Rawn, D. Mandrus, R. Jin, J. C. Bryan, Polymorphism, phase transitions, and thermal expansion of $K_3Lu(PO_4)_2$, J. Alloys Compd. 588 (2014) 182–189.
[28] Y. Ou, W. Zhou, P. Dorenbos, H. Liang, Cationic effects on photo- and X-ray radioluminescence of $K_3RE(PO_4)_2$:Ce^{3+}/Pr^{3+} (RE = La, Gd, and Y) phosphors toward X-ray detection, Inorg. Chem. 62 (2023) 6181.
[29] H.B. Tisdale, M.S. Christian, G. Morrison, T.M. Besmann, K. Sun, G.S. Was, H.-C. zur Loye, Investigation of rare earth-containing double phosphates of the type $A_3Ln(PO_4)_2$ (Ln = Y, La, Pr, Nd, and Sm–Lu) as potential nuclear Waste forms, Chem. Mater. 34 (2022) 3819–3830.
[30] S.J. Duclos, C.D. Greskovich, R.J. Lyons, J.S. Vartuli, D.M. Hoffman, R.J. Riedner, M.J. Lynch, Development of the HiLight™ scintillator for computed tomography medical imaging, Nucl. Instrum. Methods Phys. Res., Sect. A 505 (2003) 68–71.
[31] C.R. Groom, I.J. Bruno, M.P. Lightfoot, S.C. Ward, The cambridge structural database, Acta Crystallogr. Sect. B Struct. Sci. 72 (2016).
[32] S. Gates-Rector, T. Blanton, The powder diffraction file: a quality materials characterization database, Powder Diffr. 34 (2019).
[33] P.Y. Poma, K.U. Kumar, M.V.D. Vermelho, K. Serivalsatit, S.A. Roberts, C.J. Kucera, J. Ballato, L.G. Jacobsohn, C. Jacinto, Luminescence and thermal lensing characterization of singly Eu^{3+} and Tm^{3+} doped Y_2O_3 transparent ceramics, J. Lumin. 161 (2015) 306–312.
[34] R.E. Muenchausen, L.G. Jacobsohn, B.L. Bennett, E.A. McKigney, J.F. Smith, J. A. Valdez, D.W. Cooke, Effects of Tb doping on the photoluminescence of Y_2O_3:Tb nanophosphors, J. Lumin. 126 (2007) 838–842.
[35] G.F. Knoll, Radiation Detection and Measurement, John Wiley & Sons, 2000.
[36] J.H. Hubbell, S.M. Seltzer, Tables of X-ray mass attenuation coefficients and mass energy-absorption coefficients, NIST Stand. Ref. Database 126 (1995).
[37] A. Lempicki, A.J. Wojtowicz, E. Berman, Fundamental limits of scintillator performance, Nucl. Instrum. Methods Phys. Res., Sect. A 333 (1993) 304–311.
[38] L.G. Jacobsohn, A. Toncelli, K.B. Sprinkle, C.J. Kucera, J. Ballato, Spectral engineering of LaF_3:Ce^{3+} nanoparticles: the role of Ce^{3+} in surface sites, J. Appl. Phys. 111 (2012).
[39] A.A. Trofimov, C. Li, K.S. Brinkman, L.G. Jacobsohn, Luminescence investigation of Ce incorporation in garnet-type $Li_7La_3Zr_2O_{12}$, Opt. Mater. 68 (2017) 7–10.
[40] A.A. Trofimov, L.G. Jacobsohn, Radioluminescence of $Lu_3Al_5O_{12}$:Ce single crystal and transparent polycrystalline ceramic at high temperatures, Ceram. Int. 46 (2020) 26335–26338.
[41] S.V. Ushakov, A. Navrotsky, J.M. Farmer, L.A. Boatner, Thermochemistry of the alkali rare-earth double phosphates, $A_3RE(PO_4)_2$, J. Mater. Res. 19 (2004) 2165–2175.